Sustainable Environment Research

RESEARCH

Open Access

Performance and control of a reverse osmosis unit integrated with Pelton Wheel to supply emergency electric loads under various operating conditions

Fadl A. Essa[1*], F. Selim[2] and Mahmoud S. El-Sebaey[3]

Abstract

Nowadays, the whole world is moving very quickly into the field of seawater desalination. This is because the world suffers from a lack of potable water. Water and energy are adjoining linked fields. The present work aims at investigating the performance of a reverse osmosis (RO) plant integrated with Pelton Wheel under various operating conditions. The main reason for using Pelton turbine instead of the pressure exchanger (PX) is the low cost of Pelton compared to that of PX. The RO system integrated with the Pelton Wheel was tested under various operating pressures of 650, 700, 750, 800, and 850 kPa. Changing the feed water pressure affects the pressure of the reject entering the Pelton wheel and this, in turn, affects the velocity of the water jet. Also, the impact of varying the feed water salinity (total dissolved solids (TDS) = 400, 500, 600, 700, and 850 ppm) and temperature (20–39 °C) on the permeate and reject of RO was tested. In addition, a theoretical modeling was built to predict the performance of the RO system. The permeate flow rate was increased by raising the RO operating pressures. The permeate flow rate was augmented from 2.5 to 4.3 L min^{-1} when increasing the operating pressure from 650 to 850 kPa, respectively. Therefore, the permeate flow rate is enhanced by around 72% when increasing the operating pressure by only 30%. Besides, increasing the pressure by 30% (from 650 to 860 kPa) decreased the generated power of the Pelton Wheel by approximately 72% (from 960 to 270 W, respectively). Also, increasing the feed water salinity leads to raise the salinity of RO permeate, and vice versa. The RO permeate salinity is raised from 165 to 285 ppm when increasing the operating pressure from 650 to 850 kPa, respectively. As well, the more the increase in feed water temperature, the more improve in the permeate flux and salinity. The permeate TDS was decreased from 140 ppm at feed-water temperature 20 °C to 56 ppm at feed water temperature 39 °C. In this study, the Arduino program circuit was used to supply the required emergency loads by controlling the pressure values of high-pressure pump due to easy and open code program. Finally, the theoretical modelling results are in good correspondence with the experimental results. The average deviation among the theoretical and experimental results was 3.5%.

Keywords Reverse osmosis, Energy recovery system, Pelton Wheel, RO Modelling, Emergency electric loads

1 Introduction

The availability of water in communities is one of the main reasons for their survival [1, 2]. In addition, it was reported that there were 2.3 billion people having water-stressed issues with 733 million people facing critical-water stressed problems [3, 4]. In the last century, it has

*Correspondence:
Fadl A. Essa
fadlessa@eng.kfs.edu.eg
Full list of author information is available at the end of the article

been reported that water is being consumed at a rate almost twice the rate of population growth [5]. Also, the rapid development in agricultural technology, industry and medical equipment has exacerbated the water shortage problem [6–8]. In many places around the world, various desalination methods are used to overcome the problem of water shortage [9–13]. Reverse Osmosis (RO) technology and thermal distillation techniques are the well-known categories of desalination plants. Unlike the thermal distillation techniques, the RO systems have the advantages of small-horizontal space for infrastructure, simplicity for operation, low chemical constraints, simple procedures for operation, station compactness, capability of desalinating either saline, brackish, or geothermal waters, and selective separation [14, 15]. Another feature that distinguishes the RO method from other methods is its economics in operation and production [16], which facilitates its spread in all commercial societies unlike the other distillation techniques [17, 18].

The parameters affecting the performance of RO unit are the operating pressure, feed salinity, water flux, feed pH, permeate recovery ratio, and temperature of feed water. Ansari et al. [19] evaluated the performance of 50 m^3 d^{-1} RO unit with varying the input parameters of pressure and salinity. Pressure was varied between 500 and 1300 kPa, and salinity varied from 1000 to 5000 ppm. Results obtained that the performance greatly depends on the feed pressure and feed salinity. The increase of pressure at constant salinity leads to a linear rise in the flow of permeate. Also, salt rejection is decreased nonlinearly with the increase of feed water salinity. The relation between the flow rate and salinity is linear. Al-Jeshi et al. [20] investigated the effect of pressure on the performance of RO membrane in water containing 50% oil. The applied feed pressure varied from 80 to 160 MPa. The authors observed that the increase in feed pressure increases the rate of permeation, leading to oil dilution and increasing the product water flow. In addition, Shaaban et al. [21] designed, constructed and tested a typical RO system in hot climate conditions. They used ROSA software to analyze seven various membrane elements when applying a pressure varying from 260 to 600 kPa. Results showed that the osmotic pressure is increased by increasing feed water salinity. Increasing feed pressure and decreasing salinity increase permeate flux. Moreover, Kim et al. [22] investigated the applicability of a two-stage seawater RO system in the Arabian Gulf regard to the extreme conditions such as high temperature (from 20 to 40 °C) and salinity (from 30,000 to 60,000 mg L^{-1}) for a water capacity of 10,000 m^3 d^{-1}. It was found that the achieved recovery increased from 31 to 34%, although the system was used under extreme conditions. Therefore, a linear relationship was concluded between the water flux and feed pressure of RO unit [23]. In addition, a nonlinear-direct relationship was concluded by Shamel and Chung [24] between the feed pressure and salt rejection of RO unit. They also reported that the permeated flux of RO unit is proportional with the feed water temperature. Moreover, Jin et al. [25] tested the performance of RO membranes for treating brackish water under various operating temperatures of 15, 25 and 35 °C. They reported that raising the feed water temperature led to reducing the solute concentration polarization and improved the water and salt permeability. Also, the consumed power was reduced by raising the feed water temperature. Besides, Mohammed et al. [26] investigated the influence of temperature on performance of RO membrane with regard to time. The applied temperatures varied among 25, 35 and 45 °C. It was observed that salt rejection was decreased by the increase of feed water temperature. That is because of the decrease of feed solution viscosity that results in decrease in the fouling on the membrane surface. Additionally, Odabasi et al. [27] analyzed the effect of several parameters on the performance of RO membrane processes using some machine learning techniques. One of these parameters was the feed flow rate. It was found that there was an interconnected relationship between feed flow rate and permeate flow rate. High flow rate was desired for more efficient RO membrane operations. Furthermore, Ali et al. [28] simulated the integrated membrane desalination with RO membrane. Several configurations of hybrid systems including cascading and brine recycling were investigated. The performance was improved due to increasing the recovery rate and reducing the energy consumption. The water recovery ratio varied between 30 to 40% when the operating pressure of RO varied from 600 to 4000 kPa. The recovery ratio was also improved through the brine recycling. The water recovery ratio reached 90%, however it encountered the increased cost. Generous et al., [29] investigated a design model to study the performance of RO membrane. The effect of recovery ratio on the model performance was conducted. As a result, when the recovery ratio is increased, the cost of product water is decreased. Cost was observed to be reduced by 28% when recovery ratio is increased from 30 to 50%.

Therefore, the best performance of a RO unit can be achieved by integrating the unit of a PX (pressure exchanger), which is used as an excellent energy recovery system (ERS). However, the PX is expensive, especially for the remote areas and poor people. Consequently, the main aim of the present work is to investigate the performance of the RO plant integrated with a Pelton Wheel under various operating conditions. This is to obtain the performance of the proposed system to be used for remote areas and poor people with large families. The

cost of the Pelton turbine is marginal as compared to that of the PX ERS. The proposed RO system integrated with the Pelton Wheel was evaluated under various operating pressures of 650, 700, 750, 800, and 850 kPa. Changing the feed water pressure affects the pressure of the reject entering the Pelton wheel and this, in turn, affects the velocity of the water jet. The plant was operated with several pressures and measured the voltage and current generated by the Pelton wheel using a Watt meter to indicate the resulting power. Also, the impact of varying the feed water salinity (total dissolved solids (TDS) = 400, 500, 600, 700, and 850 ppm) on the permeate and reject was assessed. Additionally, the influence of the various temperatures of feed water on the permeate salinity was studied. Finally, an automatic control system (by Arduino Program Circuit) was incorporated to the system to control the electric power generated to supply emergency loads or storage the power through batteries related to the permeate flow rate of water.

2 Preparation, assembly, and testing methodology

As well-known, the RO plant consists of a low-pressure pump, high-pressure pump, RO membrane, recovery system, and auxiliary measuring and controlling instruments such as the pressure switches, valves, flow meters, Arduino circuit…etc. The recovery system utilized was a Pelton Wheel. A photograph of the tested RO plant is illustrated in Fig. 1.

The used RO membrane was a polyamide composite membrane. It is characterized by low operating pressure, higher flow, and improved desalination. It is employed in drinking water treatment plants in municipal drinking water supply, various industrial water purification, seawater desalination project, etc.

Firstly, the DuPont RO membrane 4021 is installed in its housing according to the direction of the flow. Then, the end caps are installed for the feed side and the end side. The inlet of the membrane is coming from the high-pressure pump. The output is divided into permeate and reject. In addition, the dual media was filled with gravel, sand, and coal. These three materials occupied almost two-thirds of the media filter. It is installed after the low-pressure pump and before the cartridge filter. When operating for the first time, the membrane is separated, and the device is turned on to wash the media filter. A cartridge filter of the type of the spun bonded filter cartridge was selected for more pre-filtration process. It is a piece of tubular filtration equipment that can be used in several applications for an array of filtration requirements. A cartridge is encased within a housing or a casing and used to remove unwanted particles, pollutants, and chemicals from liquids. Spun Bonded Cartridge filters (Filter Concept) are manufactured through a process that thermally bonds pure Polypropylene microfibers with lower density at the outside surface and progressively higher density toward the center. Water goes through the filter matrix and retains the particles inside the matrix that have higher efficiency and longer filters life. The Cartridge filter is installed after the media filter and before the high-pressure pump.

Fig. 1 Photograph of the investigated RO unit with ERS of Pelton Wheel

Moreover, three types of pumps are used for the purpose of operating the entire system: high pressure pump, low pressure pumps, and two dosing pumps. A low-pressure pump is used in order to withdraw feed water and deliver it to the media filter. High pressure pump is used in our project to increase the pressure of water stream before entering the RO membrane. The installed high-pressure pump is a peripheral electric pump with compact dimensions, and it is controlled (pressure values) by Arduino circuit to control the output of generated electric power. The motor is a closed asynchronous type with external ventilation cooling. The rotor is running on permanently lubricated ball bearings, oversized to ensure low noise and durability. For the protection of the three-phase motor, a remote overload cut-out was used.

A dosing pump is a positive displacement pump that is designed for the purpose of injecting a chemical substance into the flow of water, gas, or any other fluid. Two pulse injection diaphragm pumps (dosing pumps) were used for the purpose of injecting doses of chlorine and antiscalant from the dosing tanks to the stream of water. They have a controller that switches the pump on or off and controls the flow rate.

Furthermore, a solenoid valve is used as a safety valve to protect the low-pressure pump from low pressures. It prevents pressure from decreasing lower than 200 kPa. Also, a PVC (polyvinyl chloride) ball valve is used as an isolation valve for the operation of the system.

Pelton wheel is the preferred turbine for hydropower when the hydraulic head or the source of water at low

flow rates. Regarding the flow rate and pressure of the RO system, the specifications of the Pelton Wheel are designed and calculated as tabulated in Table 1. Buckets were made of PVC material with the dimensions obtained in Table 1. The length of the handle of the bucket is 2 cm and the gap between two handles is 0.75 cm. Also, the rim is made of PVC with thickness of 0.75 cm. The length of the shaft is 5.5 cm. It is made of stainless steel. Besides, the wheel casing is made of 2 mm stainless steel sheet metal. It has two holes, one for the nozzle and one for the shaft. A schematic diagram of the investigated RO unit with ERS of Pelton Wheel is shown in Fig. 2.

Table 1 Parameters and specifications of the Pelton Wheel

Parameter	Value
Speed ratio	0.44
Wheel mean diameter	20 cm
Radial length of the bucket	4.2 cm
Axial width of the bucket	6 cm
Depth of the bucket	2.2 cm
Number of buckets	12
Shaft hole diameter	1 cm
Angle between two buckets	30°

For evaluating the performance of the RO plant, suitable measuring instruments were utilized such as the TDS meter to measure the TDS of feed water, reject and permeate. Also, a Watt meter was utilized to measure the electric power generated by the Pelton wheel. A pH meter was used to measure the pH of the feed water, permeate, and reject of RO plant. In addition, the pressure gauge is used to measure the pressure in all the parts of the system, and there are inputs to Arduino circuit to evaluate the decided pressure that generates the needed electric power. Besides, a flowmeter was used to measure the flow rate of the feed water, permeate, and reject entering the Pelton wheel.

3 Experiments

The experimental tests were conducted in the labs of Kafrelsheikh University, Kafrelsheikh (31.1107° N, 30.9388° E), Egypt. The experimental test-rig was boosted by a feeding reservoir to be used for the purposes of various water salinities. Also, the brine of the desalination system was connected to the plumbing network of the lab. The experimental steps are as follows.

1. Before operating and testing the plant, the plant was switched on the washing cycle to wash the media filter. Note that this process is conducted only once in the lifetime of the media filter. After the washing

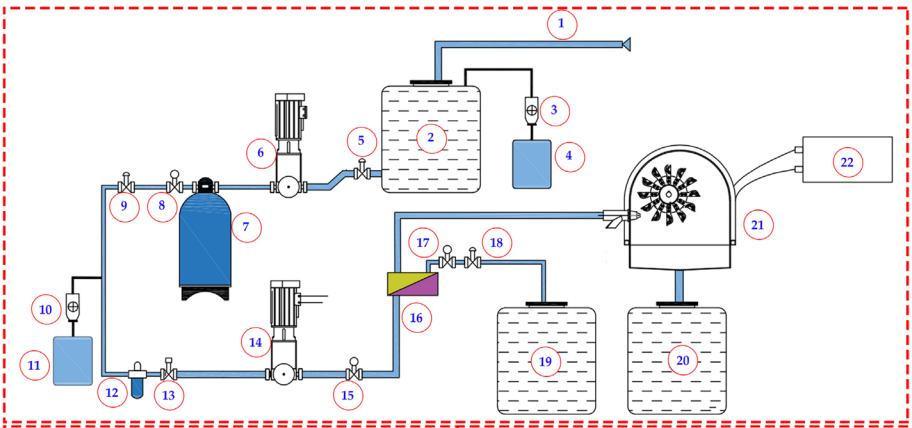

1	Feed water	12	Cartridge filter
2	Feed water tank	13	Solenoid valve
3	Dosing pump	14	High pressure pump
4	Chlorine tank	15	Pressure gauge
5	Valve	16	RO membrane
6	Low pressure pump	17	Pressure gauge
7	Media filter	18	Valve
8	Pressure gauge	19	Permeate tank
9	Valve	20	Reject tank
10	Dosing pump	21	Pelton Wheel
11	Antiscalant tank	22	Battery

Fig. 2 Schematic diagram of the investigated RO unit with ERS of Pelton Wheel

cycle, the plant is fully operated and connected to the Pelton Wheel by using the reject in operating the Pelton Wheel to generate electricity.
2. The RO system integrated with the Pelton Wheel was tested under various operating pressures from 650 to 850 kPa. The effect of varying the operating pressure on the permeate and generated power of the Pelton Wheel was investigated. Changing the feed water pressure affects the pressure of the reject entering the Pelton Wheel and this, in turn, affects the velocity of the water jet. The plant was operated with several pressures with measuring the electric power generated by the Pelton wheel using a Watt meter to calculate the resulting power.
3. Also, the impact of varying the feed water salinity (TDS from 300 to 850 ppm) on the permeate and reject was tested.
4. Additionally, the influence of the various temperatures of feed water on the permeate salinity was studied.
5. Incorporating the needed generated electric power according to on-time loads by Arduino program circuit.

Finally, the last step was flushing by the domestic water for a while to make sure that there is no concentrated solution left in the system. All tested parameters are tabulated in Table 2.

As mentioned above, the RO system was integrated with the appropriate measuring tools to be able to evaluate the plant performance. To appropriately assess the experimental data, it is critical to determine the preciseness of the observed variables. The Holman [30] approach is employed to evaluate the finding uncertainties. Table 3 shows the uncertainty of devices determined using the Holman technique.

Table 2 Steps and parameters of experiments

Testing	Parameter	Values	Unit
Step#1	Pressure, P	650	kPa
		700	
		750	
		800	
		850	
Step#2	Feed water salinity, TDS	850	ppm
		700	
		600	
		500	
		400	
		300	
Step#3	Feed water temperature	20	°C
		32.5	
		35.5	
		37.5	
		39	

4 Theoretical modelling of the RO system

In the current work, a single stage of RO membrane was tested. Figure 3 describes a schematic diagram of the tested one-stage RO unit. The feed water was forced to enter the membrane under the high pressure delivered by the high-pressure pump. The modeling equations are solved by Engineering Equation Solver (EES) software to obtain the performance of the RO unit.

Besides, the volume flow rate of the permeate (Q_p) can be found as a function of the membrane surface area A in [m^2] and the water flux of membrane J_w in [m s^{-1}] [31]:

$$Q_p = J_w.A \tag{1}$$

The water permeability "A_m" and solute transport factor are the parameters that determine the solution diffusion model for RO membrane unit, and those factors are introduced by the manufacturer. Therefore, regarding this model, the pure water flux "J_w" can be determined by [25].

$$J_w = A_m.P_{eff} \tag{2}$$

where, P_{eff} is the residual transmembrane pressure, and it is calculated by.

$$P_{eff} = \left(P_f - P_p - \Delta P_{in} - \frac{\Delta P_f}{2}\right) - \left(\pi_w - \pi_p\right) \tag{3}$$

Also, the flux of salt "J_s" equals [25].

$$J_s = B(C_w - C_p) \tag{4}$$

Where B is the solute permeability. Therefore, the pure water flux and salt flux are utilized to determine the velocity of permeate as following [32].

Table 3 Errors of measurable tools

Tool	Unit	Range	Accuracy	Error, %
Gauge pressure for LPP	kPa	0–10000	± 1	0.25
Gauge pressure for HPP	kPa	0–2000	± 0.5	0.5
Temperature sensor	°C	0–100	± 0.1	0.05
Flowmeter	L min^{-1}	0–40	± 1	1.25
TDS meter	ppm	0–1000	± 1	0.002
pH meter	-	2–14	± 0.02	0.0025
Watt meter	W	0–6000	± 1	0.25

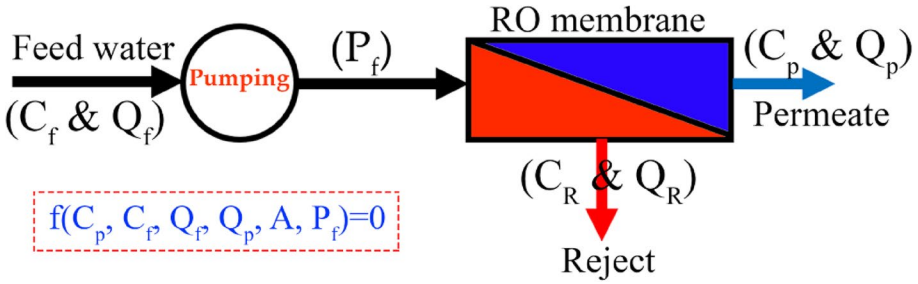

Fig. 3 Schematic diagram of the tested one-stage RO unit

$$V_w = \frac{J_w + J_s}{\rho_p} \tag{5}$$

Besides, the retentate volume flow rate is calculated by [32].

$$Q_r = Q_f - Q_p \tag{6}$$

Also, the concentration of permeate can be calculated by [32].

$$C_p = \frac{J_s}{V_w} \tag{7}$$

Hence, the membrane material balance can be formulated as [25].

$$R = 1 - \frac{C_p}{C_f} \tag{8}$$

Where R is the intrinsic or real solute rejection by the membrane. Also, the concentration of retentate can be determined by [32].

$$C_r = \frac{C_f \times Q_f - C_p \times Q_p}{Q_r} \tag{9}$$

Whilst the membrane energy balance can be formulated as.

$$P_r = P_f - \Delta P_{in} - \Delta P_{out} - \Delta P_f \tag{10}$$

However, the above relations are not yet enough to fully depict the RO membrane system. To further look into the mass transfer principles in RO membrane, the Film Theory can be referred, which considers the concentration polarization factor on the membrane feed side. Unfortunately, this concentration polarization process negatively affects the productivity of the treated water as well as the rejection of salts. In addition, it raises the osmotic pressure near the wall of the membrane more than that of the bulk feed water, and it declines the difference in net driving pressure throughout the membrane.

Therefore, the concentration on wall of membrane feed side is formulated by [32].

$$C_w = C_p + \left(\frac{C_f + C_r}{2} - C_p\right).e^{\frac{V_w}{k}} \tag{11}$$

Where C_w and C_p are the concentration of the salt at membrane surface and in bulk solution, respectively. Also, *k* is the convective mass transfer coefficient, and it can be determined by [32]

$$k = \begin{cases} 1.62 \times \left(\frac{Re \times S_c \times D_{ch}}{L_{ch}}\right)^{0.33} \times \frac{D_s}{D_{ch}} & \text{for Laminar flow } (Re \le 2100) \\ 0.023 \times (Re)^{0.875} \times (S_c)^{0.25} \times \frac{D_s}{D_{ch}} & \text{for Turbulent flow } (Re > 2100) \end{cases} \tag{12}$$

Moreover, based on the temperature, density, and salt concentration, the osmotic pressure ($\pi - Pa$) can be determined as following [32].

$$\pi(C,T) = (0.6955 + 0.0025T)10^8.\frac{C}{\rho} \tag{13}$$

It should be noted that the water flux depends mainly on the net pressure driving force across the membrane ($\Delta P - \Delta \pi$), which means the difference in the transmembrane pressure minus the difference in the osmotic pressure of the feed and permeate sides. While the salt flux relies mainly on the salt concentration difference across the membrane due to that the salt flux is the salt quantity moving through a unit membrane surface area per unit time [31].

The total pressure drop through the membrane equals the summation of the friction losses through the membrane channel (ΔP_f) and the minor losses at the inlet and outlet of membrane manifolds (ΔP_{in} and ΔP_{out}). The friction loss through the membrane channel (ΔP_f) is determined by fanning equation as following [32].

$$\Delta P_f = 2 \times f \times \rho \times V_{ch}^2 \times \frac{L_{ch}}{D_{ch}} \tag{14}$$

As well-known, the fanning friction factor (f) is determined based on the Reynolds number (Re) as following.

$$f = \begin{cases} \frac{16}{Re} & \text{for Laminar flow (Re} \le 2100) \\ \frac{0.0791}{Re^{0.25}} & \text{for Turbulent flow (Re} > 2100) \end{cases} \quad (15)$$

Also, the seawater density is approximated by.

$$\rho = 498.4 \times m + \sqrt{248400 \times m^2 + 752.4 \times m \times C} \quad (16)$$

where

$$m = 1.0069 - 2.757 \times 10^{-4} \times T \quad (17)$$

In addition, the seawater viscosity (μ) in Pa.s equals:

$$\mu = 1.234 \times 10^{-6} \times e^{\left(0.00212 \times C + \frac{1965}{T+273.15}\right)} \quad (18)$$

Besides, seawater diffusivity (D_s) in $m^2\ s^{-1}$ equals [32].

$$D_s = 6.725 \times 10^{-6} \times e^{\left(0.1546 \times 10^{-3} \times C + \frac{2513}{T+273.15}\right)} \quad (19)$$

Moreover, the minor losses at inlet and outlet of membrane pipelines (ΔP_{in} and ΔP_{out}) are considered as a minor loss of expansion from feed pipe to membrane shell and contraction from membrane shell to membrane pipe, respectively. Therefore, minor pressure drops for expansions (ΔP_{ex}) and contractions (ΔP_{co}) equal [32].

$$\Delta P_{expansion} = \left(1 - \frac{A_1}{A_2}\right)^2 \cdot \frac{V^2 \times \rho}{2 \times \alpha} \quad (20)$$

And [32],

$$\Delta P_{contraction} = 0.55 \times \left(1 - \frac{A_1}{A_2}\right)^2 \cdot \frac{V^2 \times \rho}{2 \times \alpha} \quad (21)$$

where [32]

$$\alpha = \begin{cases} 0.5 & \text{for Laminar flow (Re} \le 2100) \\ 1 & \text{for Turbulent flow (Re} > 2100) \end{cases} \quad (22)$$

By modifying Eqs. (20, 21 and 22), the inlet pressure drop for the tubular module equals.

$$\Delta P_{in} = \left[\left(1 - \frac{A_p}{A_{sh}}\right)^2 V_p^2 + 0.55\left(1 - \frac{n \times A_{ch}}{A_{sh}}\right)^2 V_{ch}^2\right] \cdot \frac{\rho}{2 \times \alpha} \quad (23)$$

And, the outlet pressure drop for the tubular module equals.

$$\Delta P_{out} = \left[\left(1 - \frac{n \times A_{ch}}{A_{sh}}\right)^2 V_{ch}^2 + 0.55\left(1 - \frac{A_p}{A_s}\right)^2 V_p^2\right] \cdot \frac{\rho}{2 \times \alpha} \quad (24)$$

As the efficiency of high-pressure pump (η_{hpp}) is 75% (from the manufacturer data sheet), the required power by the pump equals [33].

$$W_p = Q_i \times \frac{P_{out} - P_{in}}{\eta_{hpp}} \quad (25)$$

A flow chart of the theoretical solution processing is illustrated in Fig. 4. This chart presents the steps of the theoretical modeling solution obtained by EES software.

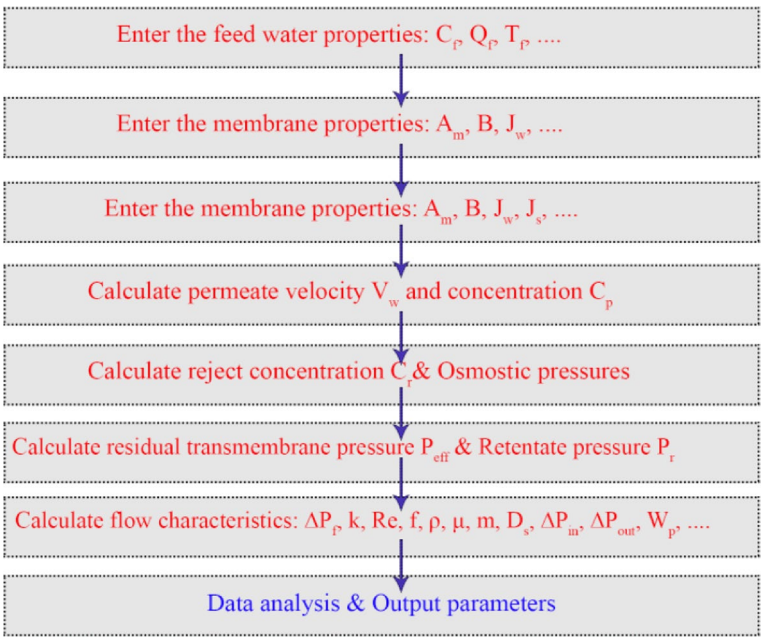

Fig. 4 Flow chart of the theoretical solution processing

Also, the constant values of parameters in the theoretical modeling are presented in Table 4.

5 Results and discussion

5.1 Validation of the theoretical modeling with experimental results

The above mathematical equations were solved by EES, and their results were compared to the experimental ones to obtain the reliability of the developed model. Figure 5 illustrates a comparison between the experimental and theoretical results of the permeate flow rate under various operating pressures. It shows that the theoretical modelling results are in a good correspondence with the experimental results. The average deviation among the theoretical and experimental results was calculated as 3.5%.

5.2 Effect of pressure on permeate flow rate

Figure 6 demonstrates the effect of the various operating pressures of the RO system on the flow rates of permeate and reject water. It is observed from Fig. 6 that the permeate flow rate was increased by increasing the operating pressures of RO system. For instance, the permeate flow rate was augmented from 2.5 to 4.3 L min^{-1} when increasing the operating pressure from 650 to 850 kPa. Therefore, the permeate flow rate is enhanced by around 72% when increasing the operating pressure by only 30%. These values obtain the importance of changing the operating pressure of the RO system. This reason behind this process maybe that the higher the operating pressure, the higher flow rate passing through the membrane module, the higher velocity of the water through the membrane and system. This process enhances the mass transfer coefficient. Therefore, the flow rate of permeate is increased. While the flow rate of retentate is declined. So, the flow rate of reject was declined from 14 to 7.6 L min^{-1} when increasing the operating pressure from 650 to 850 kPa. Therefore, increasing the operating pressure by 30% declined the reject flow rate by around 45%.

Table 4 Constant values of parameters in the theoretical modeling

Parameter	Value	Unit
η_{hpp}	75	%
A_m	2.21 10^{-9}	m CB s^{-1} kPa^{-1}
Membrane Recovery rate	15	%
Membrane area (A)	2.8	m^2
Membrane flow rate of	8	m^3 d^{-1}
Membrane pressure drop	100	kPa

5.3 Effect of pressure on the generated power

Figure 7 illustrates the effect of the various operating pressures of RO system on the generated power of the Pelton Wheel. It can be concluded from Fig. 7 that increasing the RO operating pressure decreases the generated power of the Pelton Wheel. For example, the generated power by the Pelton Wheel was 960 W at the RO operating pressure 650 kPa. While the Pelton Wheel

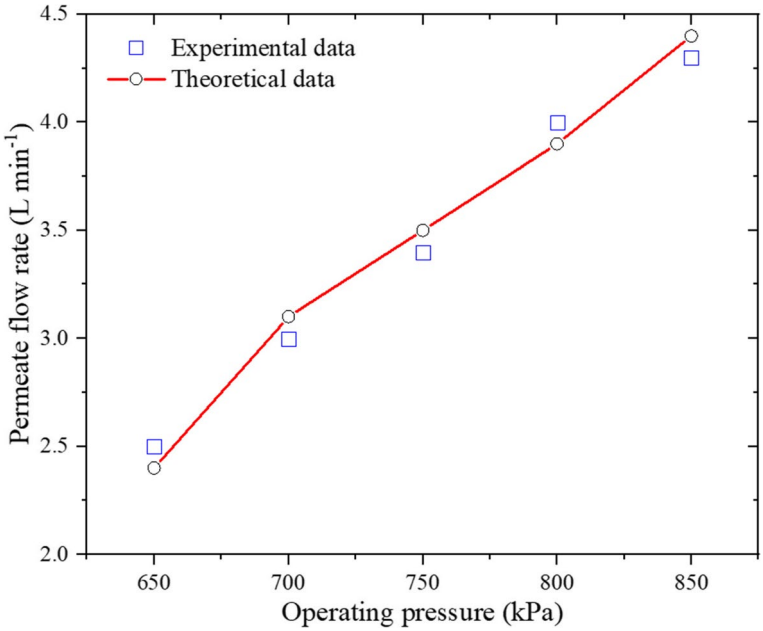

Fig. 5 Comparison between the experimental and theoretical results of the permeate flow rate under various operating pressures

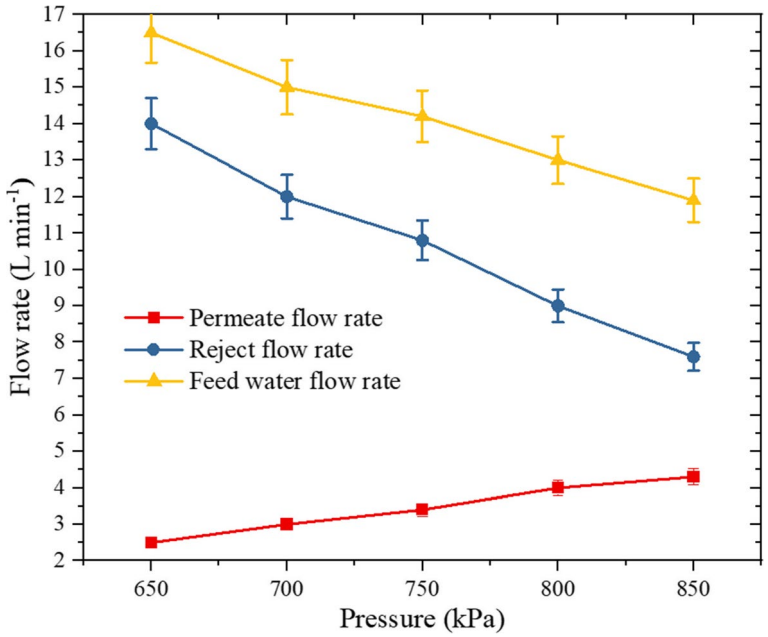

Fig. 6 The effect of the various operating pressures of RO system on the flow rates of permeate and reject water

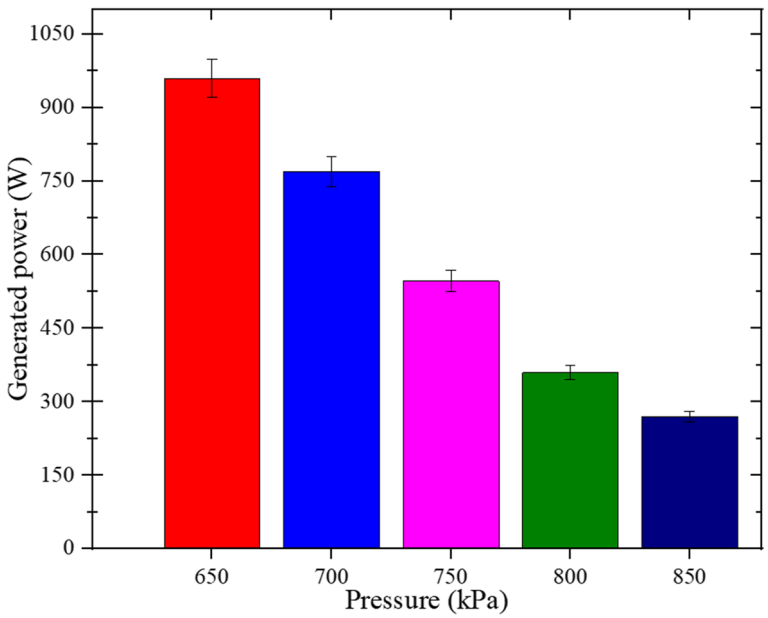

Fig. 7 The effect of the various operating pressures of RO system on the generated power of the Pelton Wheel

power was reduced to 770 W with increasing the pressure to 700 kPa. Also, raising the RO pressure from 750 to 850 kPa led to decline the generated power of the Pelton Wheel from 546 to 270 W. Therefore, it can be concluded that increasing the RO operating pressure by around 30% (from 650 to 850 kPa) decreased the generated power of the Pelton Wheel by approximately 72% (from 960 to 270 W). As a result, it can be reported that percentage of decrease in the generated power of the Pelton Wheel is almost the same percentage of increase in permeate flow rate when implementing the same percentage of increase in pressure as observed from Figs. 6 and 7. The reason behind decreasing the generated power of the Pelton Wheel can be explained regarding

the following phenomenon. Increasing the RO operating pressure improves the permeate flow rate and reduces the flow rate of reject. As explained in Sect. 3 (Experiments), the Pelton Wheel is fed by the retentate of the RO unit. So, the lower the reject flow rate of the RO unit, the lower the flow rate of water entering the Pelton Wheel, and vice versa. As increasing the RO operating pressure raised the permeate flow rate and reduced the retentate flow rate of the RO system, increasing the RO operating pressure reduced the water flow rate entering the Pelton Wheel. In addition, the power of the Pelton Wheel depends mainly on the water flow rate entering it. Therefore, reducing the flow rate of water entering the Pelton Wheel leads to decrease the power generated by it. So, increasing the RO operating pressure leads to reduce the generated power by the Pelton Wheel as illustrated in Fig. 7.

5.4 Effect of feed water salinity on the permeate and reject TDS

Figure 8 demonstrates the effect of the various feed water salinities on the permeate salinity under fixed operating pressure of 650 kPa. The salinity of feed water was ranged between 400 to 850 ppm (Fig. 8). The low feed water salinity was tested under various values to match the specifications of the membrane module of the RO unit. It can be concluded from Fig. 8 that increasing the feed water salinity leads to increased salinity of the RO permeate, and vice versa. For example, the salinity of the RO permeate is raised from 165 to 240 ppm when increasing the feed water salinity from 400 to 600 ppm, respectively. Also, raising the feed water salinity from 700 to 850 ppm leads to raise the salinity of the RO permeate from 270 to 285 ppm, respectively. As well, it can be concluded that the feed water salinity strongly affects the salinity of both permeate and retentate of the RO system. The higher the feed water salinity, the more the salinity of both permeate and retentate as shown in Fig. 8.

5.5 The effect of temperature on the permeate TDS

The temperature of RO feeding water was ranged from 20 to 39 °C. Figure 9 illustrates the effect of the various feed water temperatures on the permeate salinity under a fixed operating pressure of 650 kPa. It is revealed from Fig. 9 that the higher in feed water temperature, the more decrease in the permeate TDS. This is because raising the feed water temperature reduces declines the concentration of salt on the membrane surface. For instance, the permeate TDS was decreased from 140 ppm at feed water temperature 20 °C to 56 ppm at feed water temperature 39 °C as shown in Fig. 9. This can be explained as the water physical properties varies with change in temperature, hence the mass transfer coefficient would be changed. As the feed water temperature raises, the mass transfer coefficient is increased, and concentration of salt is declined.

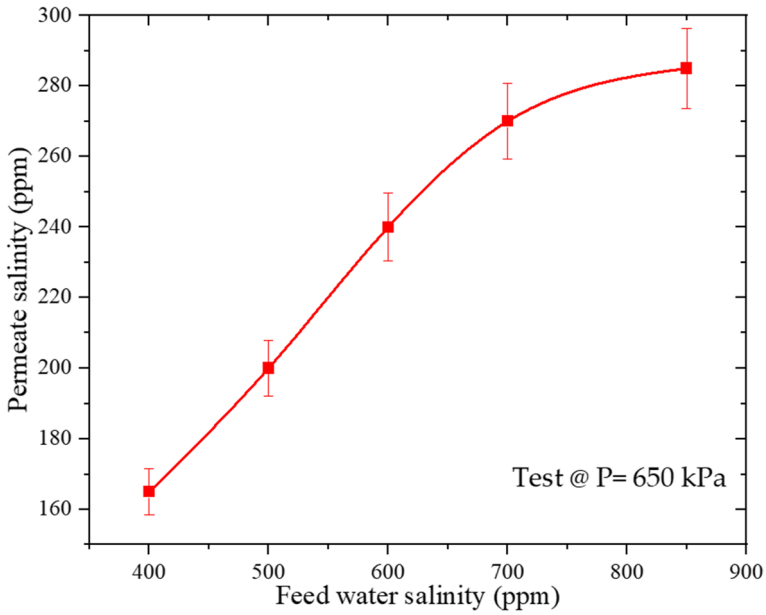

Fig. 8 The effect of the various feed water salinities on the permeate salinity under fixed operating pressure

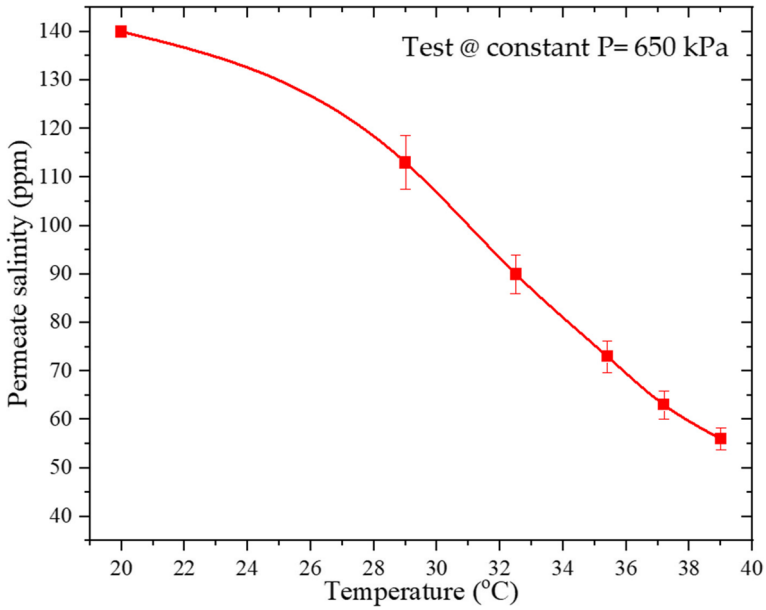

Fig. 9 The effect of the various feed water temperatures on the permeate salinity under fixed operating pressure

5.6 Control of generated electric power by Arduino program

As shown through Figs. 6 and 7, the effect of the various operating pressures of RO system on the generated power and permeate flow rate is the reverse effect. The user of this system can use the generated power to supply loads (e.g. emergency loads) through on-line supply or battery storage as renewable energy source. For example, authors use hydraulic power and photovoltaic to generate clean and natural electrical power resources to supply an emergency loads or limited the consumed electrical energy bill to a certain acceptable economic strip as in [34]. As illustrated in the above sections, the pressure of high-pressure pump is the key to decide the outputs of the permeate flow rate and generated electrical power. Therefore, according to user priority (e.g. increasing the generated power rather than permeate flow rate or vice versa), the pressure should be set (adjust) to give this needed power. The system can be controlled by using proposed Arduino circuit which controls the pressure, high pressure pump, to any values by its open code program as shown in Fig. 10. The Arduino program circuit is very simple and recommended usage for these cases to generate electric power. Its operation depends on three sensor inputs; one from pressure point in the water outlet from high pressure pump, the second and third sensors are to measure the current and voltage of the actual emergency load (needed power). For any needed values (generated power or permeate flow), the Arduino software program can decide the required outlet pressure from high pressure pump, and it can control the setting by ON/Off relay, which in turn can operate On/Off of circuit breaker of high pressure pump. There are two control types; the first is the Arduino program that sets the operation of high-pressure pump according to the inputs of needed loads (current and voltages), in the second control the user will adjust the setting pressure and then the Arduino operates high pressure pump according to this setting. For example, if the user needs the generated power, supplied emergency loads, to be 960 W (second control type) then the Arduino program will automatically set the pressure state of high-pressure pump to be 650 kPa and it adjusts its circuit breaker On/Off operation to this value and so on.

According to Ref. [34], water in motion possesses three forms of energy; kinetic energy due to its velocity, pressure energy due to its pressure, and potential energy due to its height. The used type in this study is pressure one with energy:

$$Pressure\ energy = \frac{Pi}{\rho} \tag{26}$$

where:

P*i* is inlet water pressure to Pelton Wheel turbine, N m^{-2}

p is the density of water, kg m^{-3}

6 Conclusions

In this study, the performance of a RO plant integrated with a Pelton Wheel under various operating conditions of various operating pressures (650–850 kPa), various feed water salinity (TDS = 400–850 ppm), and various

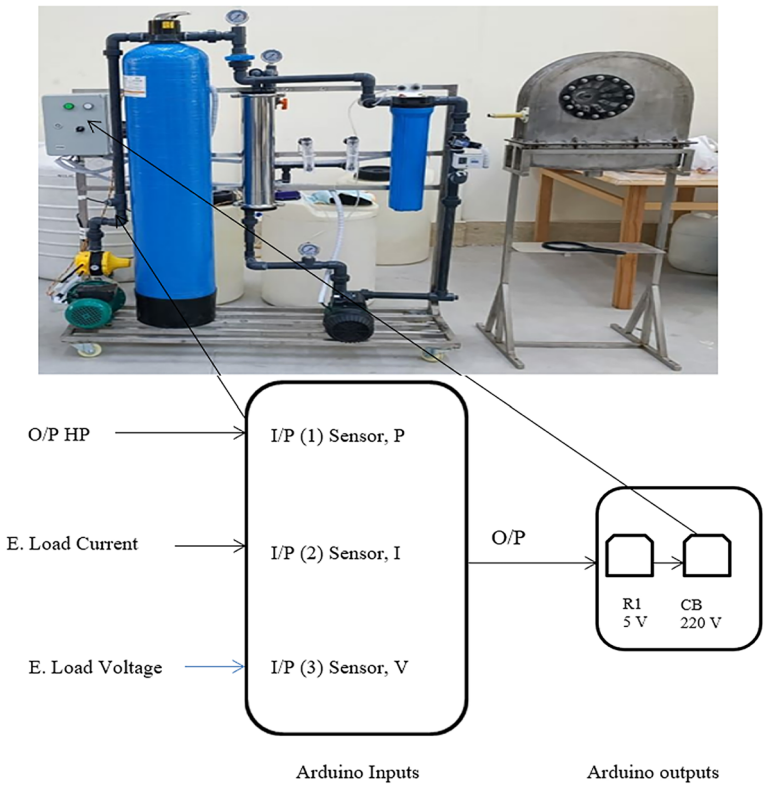

Fig. 10 Arduino Circuit for control the pressure and generated electric power

temperatures of feed water (20–39 °C). The following points can be concluded based on the above results. The permeate could be increased by raising the operating pressure of RO system. For instance, the flow rate of permeate was augmented from 2.5 to 4.3 L min^{-1} when increasing the operating pressure from 650 to 850 kPa. Therefore, the permeate flow rate is enhanced by around 72% when increasing the operating pressure by only 30% (from 650 to 850 kPa). In addition, increasing the RO operating pressure decreases the generated power of the Pelton Wheel. For example, the generated power by the Pelton Wheel was reduced from 960 W at 650 kPa to 270 W at 850 kPa. Therefore, increasing the pressure by 30% (from 6.5 to 850 kPa) decreased the generated power of the Pelton Wheel by approximately 72% (from 960 to 270 W). Moreover, the Arduino program circuit could be a simple tool to supply the required emergency loads by controlling the pressure values of high-pressure pump due to easy and open code program. The Arduino circuit can be programmed to compare the priority of generating either the permeate flow rate or electric generated power, they are with reverse effect, according to needs and cost analysis. Furthermore, increasing the feed water salinity leads to raise the salinity of the RO permeate, and vice versa. For example, the salinity of the RO permeate is raised from 165 to 285 ppm when increasing the operating pressure from 650 to 850 kPa. Finally, the more increase in feedwater temperature, the more decrease in the permeate TDS. For instance, the permeate TDS was decreased from 140 ppm at feedwater temperature 20 °C to 56 ppm at feedwater temperature 39 °C.

7 Nomenclatures

A_m Water permeability, md
C_p Concentration of permeate, %
C_r Concentration of retentate, %
C_w Concentration on wall of membrane feed side, %
D_s Seawater diffusivity, $m^2\ s^{-1}$
J_s Flux of salt, $m\ s^{-1}$
J_w Water flux of membrane, $m\ s^{-1}$
P_{eff} Residual transmembrane pressure, kPa
Q_p Volume flow rate of the permeate, $m^3\ s^{-1}$
Q_r Retentate volume flow rate, $m^3\ s^{-1}$
V_w Velocity of permeate, $m\ s^{-1}$
W_p Pump power, W
η_{hpp} Efficiency of high-pressure pump, %
ΔP_f Friction losses, kPa
ΔP_{in} Minor losses at the inlet of membrane manifolds, kPa

ΔP_{out} Minor losses at the outlet of membrane manifolds, kPa
A Membrane surface area, m^2
B Solute transport factor
R Intrinsic or real solute rejection by the membrane
Re Reynolds number
T Temperature, °C
f Fanning friction factor
k Convective mass transfer coefficient
m Mass, kg
μ Seawater viscosity, Pa s
π Osmotic pressure, kPa
ρ Density, kg m^{-3}

Authors' contributions
Fadl Abdelmonem Essa: Conceptualization, Methodology, Writing—original draft preparation, Editing, and Formal analysis. F. Selim: Formal analysis, Writing, Review, and Explanation, Editing. Mahmoud S. El-Sebaey: Response to reviewer comments, English editing, Explanation.

Funding
Open access funding provided by The Science, Technology & Innovation Funding Authority (STDF) in cooperation with The Egyptian Knowledge Bank (EKB). No funding for this work.

Availability of data and materials
Not applicable.

Declarations

Ethics approval and consent to participate
Not applicable.

Consent for publication
Not applicable.

Competing interests
No competing interests.

Author details
[1]Mechanical Engineering Department, Faculty of Engineering, Kafrelsheikh University, Kafrelsheikh 33516, Egypt. [2]Electrical Engineering Department, Faculty of Engineering, Kafrelsheikh University, Kafrelsheikh 33516, Egypt. [3]Mechanical Power Engineering Department, Faculty of Engineering, Menoufia University, Shebin El-Kom 32511, Egypt.

Received: 21 March 2023 Accepted: 9 July 2023
Published online: 01 August 2023

References

1. Essa FA. Thermal Desalination Systems: From Traditionality to Modernity and Development. In: Steffen V, editor. Distillation Processes - From Solar and Membrane Distillation to Reactive Distillation Modelling, Simulation and Optimization. London: IntechOpen; 2022.
2. Panchal H, Nurdiyanto H, Sadasivuni KK, Hishan SS, Essa FA, Khalid M, et al. Experimental investigation on the yield of solar still using manganese oxide nanoparticles coated absorber. Case Stud Therm Eng. 2021;25:100905.
3. UN Water. Summary Progress Update 2021: SDG 6 — water and sanitation for all. Geneva: United Nations Water; 2021
4. Essa FA, Omara ZM, Abdullah AS, Shanmugan S, Panchal H, Kabeel AE, et al. Wall-suspended trays inside stepped distiller with Al_2O_3/paraffin wax mixture and vapor suction: Experimental implementation. J Energy Storage. 2020;32:102008.
5. Abdullah AS, Omara ZM, Essa FA, Alqsair UF, Aljaghtham M, Mansir IB, et al. Enhancing trays solar still performance using wick finned absorber, nano- enhanced PCM. Alex Eng J. 2022;61:12417–30.
6. Salehi M. Global water shortage and potable water safety; Today's concern and tomorrow's crisis. Environ Int. 2022;158:106936.
7. El-Fakharany ZM, Salem MG. Mitigating climate change impacts on irrigation water shortage using brackish groundwater and solar energy. Energy Rep. 2021;7:608–21.
8. Essa FA, Abdullah AS, Alawee WH, Alarjani A, Alqsair UF, Shanmugan S, et al. Experimental enhancement of tubular solar still performance using rotating cylinder, nanoparticles' coating, parabolic solar concentrator, and phase change material. Case Stud Therm Eng. 2022;29:101705.
9. Elsheikh AH, Sharshir SW, Mostafa ME, Essa FA, Ahmed Ali MK. Applications of nanofluids in solar energy: A review of recent advances. Renew Sustain Energy Rev. 2018;82:3483–502.
10. Sangeetha A, Shanmugan S, Alrubaie AJ, Jaber MM, Panchal H, Attia MEH, et al. A review on PCM and nanofluid for various productivity enhancement methods for double slope solar still: Future challenge and current water issues. Desalination. 2023;551:116367.
11. Diab MR, Essa FA, Abou-Taleb FS, Omara ZM. Solar still with rotating parts: a review. Environ Sci Pollut R. 2021;28:54260–81.
12. Essa FA, Abdullah AS, Omara ZM, Kabeel AE, El-Maghlany WM. On the different packing materials of humidification–dehumidification thermal desalination techniques – A review. J Clean Prod. 2020;277:123468.
13. Abdullah AS, Omara ZM, Essa FA, Younes MM, Shanmugan S, Abdelgaied M, et al. Improving the performance of trays solar still using wick corrugated absorber, nano-enhanced phase change material and photovoltaics-powered heaters. J Energy Storage. 2021;40:102782.
14. Al-Obaidi MA, Alsarayreh AA, Al-Hroub AM, Alsadaie S, Mujtaba IM. Performance analysis of a medium-sized industrial reverse osmosis brackish water desalination plant. Desalination. 2018;443:272–84.
15. Essa FA, Elaziz MA, Al-Betar MA, Elsheikh AH. Performance prediction of a reverse osmosis unit using an optimized Long Short-term Memory model by hummingbird optimizer. Process Saf Environ. 2023;169:93–106.
16. Igobo ON, Davies PA. Isothermal Organic Rankine Cycle (ORC) driving Reverse Osmosis (RO) desalination: Experimental investigation and case study using R245fa working fluid. Appl Therm Eng. 2018;136:740–6.
17. Mateo TA. Solar Powered Desalination System [Master Thesis]. San Diego: University of California, San Diego; 2011.
18. Thamizharasu P, Shanmugan S, Gorjian S, Pruncu CI, Essa FA, Panchal H, et al. Improvement of thermal performance of a solar box type cooker using SiO_2/TiO_2 nanolayer. Silicon-Neth. 2022;14:557–65.
19. Ansari M, Al- Obaidi MA, Hadadian Z, Moradi M, Haghighi A, Mujtaba IM. Performance evaluation of a brackish water reverse osmosis pilot-plant desalination process under different operating conditions: Experimental study. Cleaner Eng and Technol. 2021;4:100134.
20. Al-Jeshi S, Neville A. An experimental evaluation of reverse osmosis membrane performance in oily water. Desalination. 2008;228:287–94.
21. Shaaban S, Yahya H. Detailed analysis of reverse osmosis systems in hot climate conditions. Desalination. 2017;423:41–51.
22. Kim J, Park K, Hong S. Application of two-stage reverse osmosis system for desalination of high-salinity and high-temperature seawater with improved stability and performance. Desalination. 2020;492:114645.
23. Ruiz-Garcia A, Nuez I, Carrascosa-Chisvert MD, Santana JJ. Simulations of BWRO systems under different feedwater characteristics. Analysis of operation windows and optimal operating points. Desalination. 2020;491:114582.
24. Shamel MM, Chung OT. Drinking water from desalination of seawater: optimization of reverse osmosis system operating parameters. J Eng Sci Technol. 2006;2:203–11.
25. Jin X, Jawor A, Kim S, Hoek EMV. Effects of feed water temperature on separation performance and organic fouling of brackish water RO membranes. Desalination. 2009;239:346–59.
26. Mohammed SA, Abbas AD, Sabry LS. Effect of operating conditions on reverse osmosis (RO) membrane performance. J Eng. 2014;20:61–70.
27. Odabasi C, Dologlu P, Gulmez F, Kusoglu G, Caglar O. Investigation of the factors affecting reverse osmosis membrane performance using machine-learning techniques. Comput Chem Eng. 2022;159:107669.

28. Ali E, Orfi J, Najib A, Saleh J. Enhancement of brackish water desalination using hybrid membrane distillation and reverse osmosis systems. Plos One. 2018;13:e0205012.
29. Generous MM, Qasem NAA, Akbar UA, Zubair SM. Techno-economic assessment of electrodialysis and reverse osmosis desalination plants. Sep Purif Technol. 2021;272:118875.
30. Holman JP. Experimental Methods for Engineers. 8th ed. New York: McGraw Hill; 2011.
31. Qasim M, Badrelzaman M, Darwish NN, Darwish NA, Hilal N. Reverse osmosis desalination: A state-of-the-art review. Desalination. 2019;459:59–104.
32. Kotb H, Amer EH, Ibrahim KA. On the optimization of RO (Reverse Osmosis) system arrangements and their operating conditions. Energy. 2016;103:127–50.
33. Di Martino M, Avraamidou S, Cook J, Pistikopoulos EN. An optimization framework for the design of reverse osmosis desalination plants under food-energy-water nexus considerations. Desalination. 2021;503:114937.
34. Selim FF, Abdelaziz A, Taha IBM. Economic design of hybrid pico-hydraulic/photovoltaic generation system: a case study in Egypt. Electronics. 2021;10:2947.

Publisher's Note